Title	Pixel-to-pixel fiber-coupled emissive micro-light-emitting diode arrays
Author(s)	Zhu, L; Ng, CW; Wong, N; Wong, KKY; Lai, PT; Choi, HW
Citation	IEEE Photonics Journal, 2009, v. 1 n. 1, p. 1-8
Issued Date	2009
URL	http://hdl.handle.net/10722/58789
Rights	Creative Commons: Attribution 3.0 Hong Kong License

Pixel-to-Pixel Fiber-Coupled Emissive Micro-Light-Emitting Diode Arrays
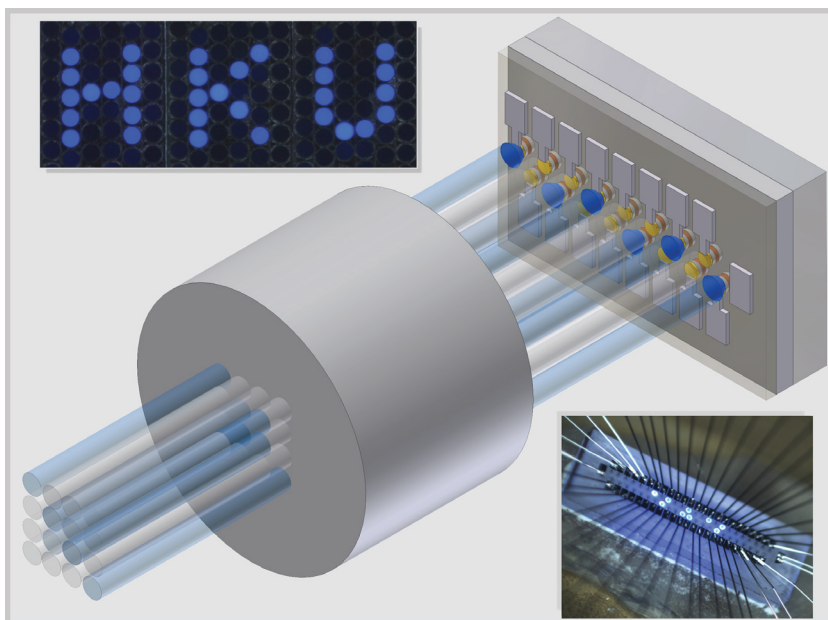
Volume 1, Number 1, June 2009

L. Zhu

C. W. Ng

N. Wong, Member, IEEE

K. K. Y. Wong, Member, IEEE

P. T. Lai, Senior Member, IEEE

H. W. Choi, Senior Member, IEEE

Pixel-to-Pixel Fiber-Coupled Emissive Micro-Light-Emitting Diode Arrays

L. Zhu, C. W. Ng, N. Wong, *Member, IEEE*, **K. K. Y. Wong,** *Member, IEEE*, **P. T. Lai,** *Senior Member, IEEE*, **and H. W. Choi,** *Senior Member, IEEE*

Department of Electrical and Electronic Engineering, University of Hong Kong, Hong Kong

Abstract: We report on an integrated fiber-coupled bi-linear micro-light-emitting diode array, serving as a portable microdisplay system. The fiber bundle transforms the bi-linearly arranged optical signals from the emissive array into a 6-by-8 pixel microdisplay, offering a crisp and clear optical output. The pixel-to-pixel coupling arrangement ensures optical coupling efficiency. Due to the narrow acceptance cones of optical fibers, individual pixels can be well resolved with minimal crosstalk. The performance and functionality of this optical system is fully evaluated. A model to determine the fiber-coupling efficiency was constructed; it was found that the simulated results compare well with the measured data.

Index Terms: GaN, micro-light-emitting diode, microdisplay, fiber coupling.

1. Introduction

The applications involving nitride-based ultra-violet or visible light-emitting diodes (LEDs) extend well beyond the typical usages as indicator lamps or general lighting; other applications have been demonstrated recently, one of which is the emissive microdisplay comprising arrays of micrometer-scale LEDs [1]. Apart from the application as microdisplays, micro-LED arrays have also been used for biological imaging and detection [2], fluorescence detection [3] and maskless lithography [4]. Most of the reported two-dimensional (2-D) micro-LED arrays are designed based on the matrix-addressing method, a strategy which reduces the overall number of bonding pads. However, the complexity of the device fabrication process is increased; so is the requirement on the driving circuitry [5]. To overcome these difficulties, we demonstrate a scheme of generating a 2-D micro-display from a bi-linear LED array via a specially-designed fiber bundle whereby fibers are linearly arranged on one end, while having a 2-D arrangement at the other. Such a one-dmensional to 2-D conversion idea is derived from round to keyed linear fiber bundles used for coupling light through the narrow slit at the entrance of a spectrograph.

The fiber bundle enables multiple optical signals to be simultaneously transmitted away from the source, eliminating the need for bulky and lossy optics as with free-space transmission [6]. At the output end, the signals can be projected for imaging purposes. Distinguishing from the use of a 30 000-channel multi-core imaging fiber in the demonstration by Xu *et al.* [7], our fiber-coupling system is further optimized, requiring just as many fiber strands as there are LED pixels without loss of resolution. Apart from imaging purposes, this fiber-coupled LED system can be adapted for multi-channel data transmission [8], a task which has traditionally been fulfilled by laser sources, or for photoexcitation of biological materials [7]. The divergent nature of LED emission results in inevitable
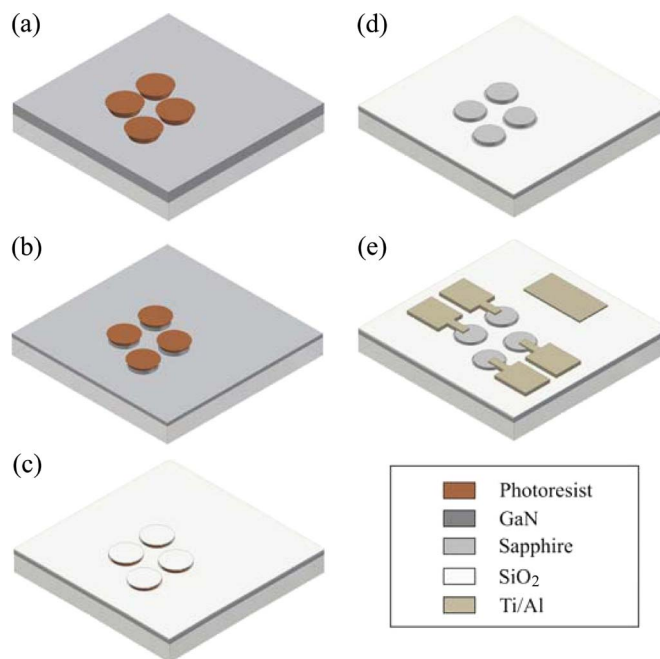
Fig. 1. 3-D schematic diagrams illustrating the fabrication process flow and the layout of the device structure: (a) patterning by image-reversal photolithography; (b) pillar structures with residual photoresist after RIE etching; (c) SiO_2 by e-beam deposition; (d) active region exposure after oxide lift-off; (e) final device structures after p- and n-pad formation.

crosstalk between adjacent pixels. In our previous works on micro-LED arrays, it was found that the light cone from adjacent pixels tend to merge at higher driving currents due to Lambertian dispersion [9], making it impossible to resolve individual pixel points. The fiber bundle eliminates crosstalk by virtue of its limited acceptance cone, ensuring that the output pattern is sharp and fully resolvable.

2. Experimental Details

Our bi-linear micro-LED array is designed with 47 pixels arranged across two rows, fabricated on an MOCVD-grown InGaN/GaN LED wafer with specified wavelength of 470 nm (blue). After depositing a Ni/Au (7 nm/7 nm) current spreading layer by e-beam evaporation system followed by rapid thermal annealing in air (550 °C, 10 mins), the microdisk active regions with different diameters (20 μm, 40 μm and 60 μm) are photolithographically defined, all with the same center-to-center spacing of 120 μm. An image-reversal photoresist (AZ-5214) was used in order to produce a T-shaped profile with overhanging lips [10] to facilitate oxide lift-off at a later stage, as illustrated in the schematic diagram in Fig. 1(a). The pillar structures were formed by reactive ion etching (RIE), as shown in Fig. 1(b). Prior to metal deposition, a 10-nm-thickness SiO_2 layer was deposited by e-beam evaporation system to act as an insulating layer, depicted in Fig. 1(c). With the residual photoresist on the active regions after etching, the top-contacts of the individual pixels are exposed by a lift-off process. The photoresist patterns with a T-shaped profile ensured effortless lift-off. After oxide lift-off, the top regions of the pillars are exposed for contacts, while the regions surrounding the pillars are protected with oxide to prevent shorting of the p-n junctions, as illustrated in Fig. 1(d). Finally, a Ti/Al (20 nm/200 nm) layer was deposited to form bonding pads, producing the final device structure of Fig. 1(e). While the pixels share two common n-contact pads located at either ends of the array (which serve to increase the current spreading uniformity in the n-GaN layer), they each have their individual p-contact pad to provide individual control. The chips are then diced by laser-micromachining and die-bonded to a 48-pin ceramic side-braze package and subsequently wire-bonded. A close-up view of the final packaged device (with pixel diameters of 20 μm) with several illuminated pixels is depicted in Fig. 2(a); Fig. 2(b) shows the far-field oblique view of the same device. The fiber
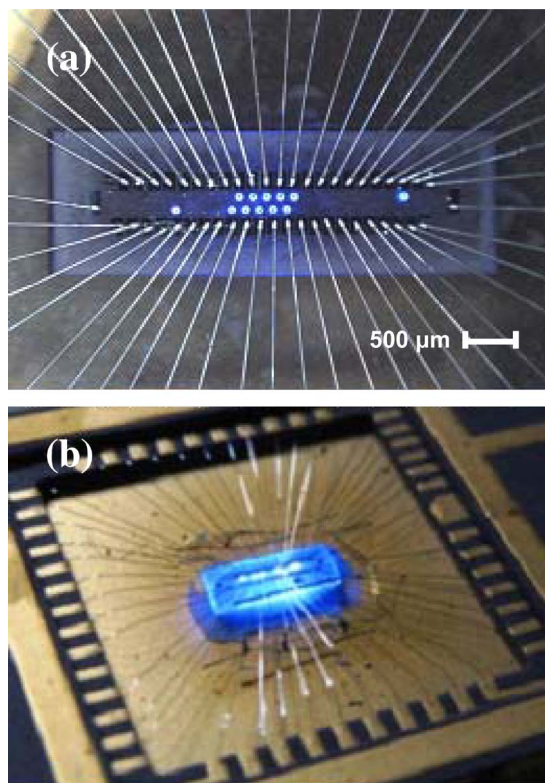
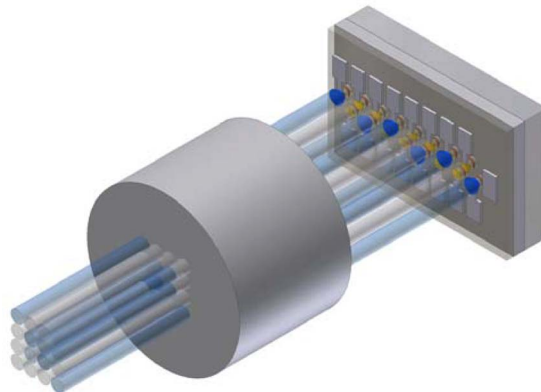Fig. 2. Operational image of the packaged micro-LED array at (a) close-up and (b) far-field oblique views.

Fig. 3. A 3-D schematic diagram showing the fiber-coupling system, highlighting the pixel-to-pixel nature of coupling between the linearly arrayed LED pixels and the fiber strands, together with fibers arranged in a 6 × 8 array at the output (exit) end.

bundle was designed such that the two ends are bi-linear and 2-D terminated, respectively. The diameter of each strand of fiber core is about 90 μm. At the input (entrance) end, the fibers are aligned such that the center-to-center spacing and arrangement is identical to that of the bi-linear micro-LED array. This arrangement allows light from each emitting pixel to effectively couple light into its corresponding fiber. The fibers are twisted along the cable to give a 6 × 8 2-D arrangement at the output (exit) end, at a resolution of ~1000 dots per inch (dpi). A three-dimensional (3-D) schematic diagram of the coupling setup, indicating the conversion from a linear-arranged input to a 2-D output, is shown in Fig. 3. Microphotographs in Fig. 4(a)–(c) depict the 24 × 2 input and 6 × 8 output ends of the bundle, together with an image of the actual fiber coupling setup.
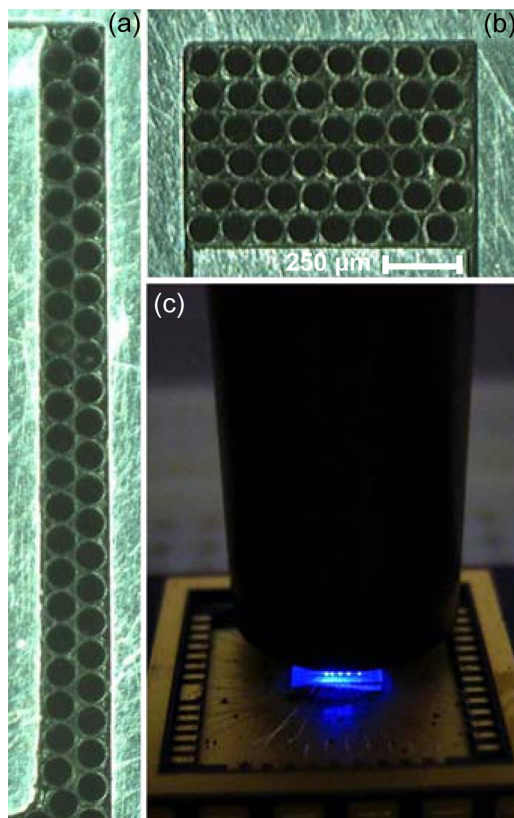
Fig. 4. Microphotographic images showing (a) the 24 × 2 input end and (b) the 6 × 8 output end of the fiber bundle and (c) the alignment of fiber bundle to the micro-LED arrays.

The device is driven by an FPGA-constructed circuit which enables alphanumeric characters to be displayed. The fiber bundle is mounted on a 3-axis micromanipulator for precise alignment to the microarray. Optimal alignment is achieved when maximum optical signal is detected at the output end. The measured turn-on voltage of the device is ~3.8 V, while the injection current at 3.3 V is 1.58 mA for each 20-μm pixel. The LEDs are operated at this voltage since they are driven by the digital output of an FPGA board. At this current, each pixel emits 26.9 μW of monochromatic light (measured with a calibrated Si photodetector placed in proximity to the device). Emission at microwatts level is due to the micrometer dimensions of the pixels. With the dual n-pad design, the pixels emit with high uniformity across a row. The functionality of the fiber-coupled micro-LED array as a microdisplay is demonstrated by displaying illuminated pixels at the 2-D end of the fiber bundle. Fig. 5 shows optical microphotographs captured from the 6 × 8 fiber array, displaying a sequence of letters "HKU," as well as the corresponding illuminated pixels on bi-linear micro-LED array. The output appears sharp and of good contrast, displaying clear and legible patterns with negligible crosstalk, attributed to the narrow acceptance cone of the fiber.

3. Results and Discussions

Efficient coupling of light into the fibers is an important consideration of this system because LEDs are emitters with radiation patterns which approximate the Lambertian distribution. As a result, it is difficult to collect most of the emitted light and guide them into the fiber cores. Fig. 6 shows a cross-sectional schematic diagram detailing the fiber-coupling arrangement. The diameter of an individual micro-LED pixel (d), the diameter of fiber core (D), together with the center-to-center spacing (W), is 20 μm, 90 μm and 120 μm, respectively. Additionally, h represents the separation between the fiber and the emitter.
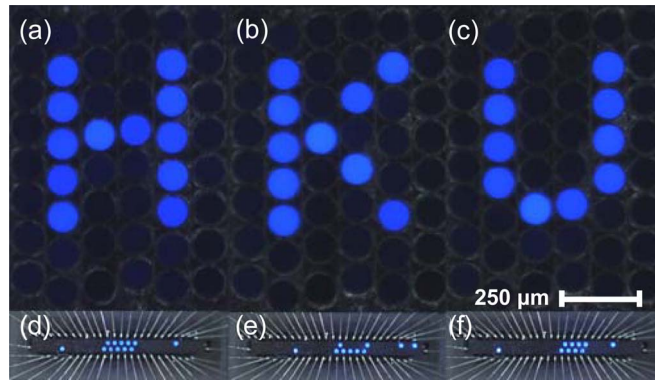
Fig. 5. (a)–(c) Optical microscope images from the exit end of the fiber, displaying the letters "HKU." (d)–(f) The corresponding illuminated pixels on the micro-LED array.
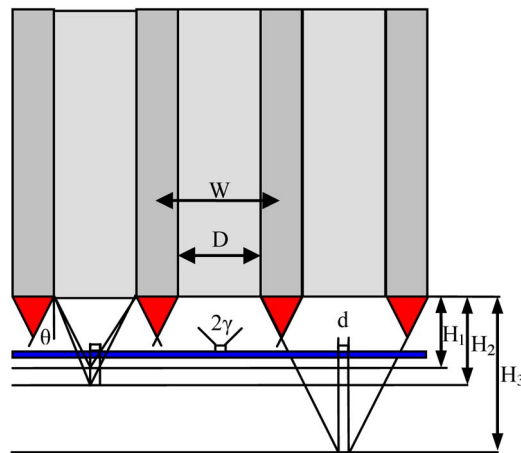

Fig. 6. Cross-sectional schematic diagram illustrating how light emitted from the micro-LEDs is coupled into the fiber.

The half-angle (θ) of 14.1° for the fiber acceptance cone can be calculated using the following equation from the numeral aperture $(NA = 0.22)$

$$NA = n_0 \sin \theta, \tag{1}$$

where the refractive index of air, n_0, is 1. The angular beam divergence (γ) of the micro-LED pixel should also be taken into account. In a report by Jiang *et al.*, a value of $2\gamma = 120°$ for a single blue micro-LED was determined from the measured angular emission distribution plot [11]. The overall coupling efficiency η, can thus be estimated using a geometrical approach with the following relation:

$$\eta = P_{fiber}/P_{LED} = \eta_{Fresnel} \times \eta_{ang}, \tag{2}$$

where P_{LED} and P_{fiber} are the optical powers before and after coupling into the fiber, while $\eta_{Fresnel}$ and η_{ang} are the Fresnel factor (taking Fresnel losses into account) and angular factor (considering angular losses), respectively. The Fresnel factor, which accounts for the losses due the difference in refractive indices between air and silica, can be approximated by

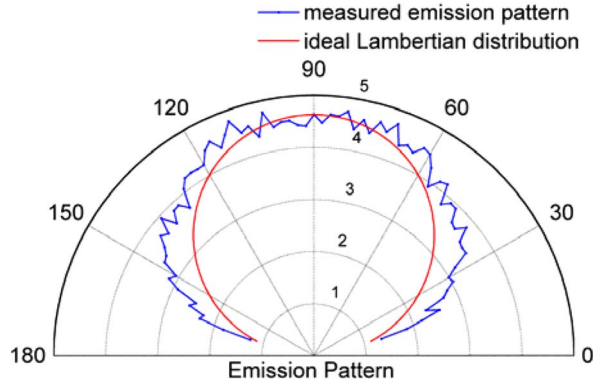$$\eta_{Fresnel} = 1 - (n_{fiber} - 1)^2/(n_{fiber} + 1)^2, \tag{3}$$

Fig. 7. A diagram shows the actual emission pattern corresponds with the ideal Lambertian distribution.

where n_{fiber}, the refractive index of the fiber core, is 1.46, giving a value of 0.96 for $\eta_{Fresnel}$. On the other hand, the inherent fiber loss can be neglected in this calculation since the transmission length of our fiber bundle is only about 1 m.

The angular emission pattern of our microsized LEDs is measured by fixating a device at the center of a rotation stage with a collection fiber placed orthogonal to the emission pixel at a separation distance of 1 cm. The stage was rotated from $14°$ to $176°$ at intervals of $2°$ (the device emission plane is set as $0°$). An optical spectrum was collected through the fiber at each point. The relative integrated optical intensities as a function of angle are plotted in Fig. 7, which illustrates the emission pattern of our micro-LEDs. The normalized Lambertian distribution function is also plotted on the same graph for comparison.

From these two plots, it is observed that the micro-LED emission pattern can be modeled as a Lambertian distribution with reasonably good accuracy. Hence, the Lambertian emission pattern for the LEDs can be described by the cosine relation:

$$I(\alpha) = I_0 \cos \alpha \ d\Omega \ dA, \tag{4}$$

where I_0 is the maximum rate of photon emission per unit solid angle along the normal direction, diminishing to zero for $\alpha = 90°$, while $I(\alpha)$ is the emission rate at an angle of α from the normal, and A is the emitting area. By performing the integrations the angular coupling efficiency factor is derived as

$$\eta_{ang} = \int_0^{\alpha_0} \sin \alpha \ \cos \alpha \ d\alpha / \int_0^{\pi/2} \sin \alpha \ \cos \alpha \ d\alpha, \tag{5}$$

where α_0 is a piecewise function dependent on the spacing h due to the fiber acceptance angle (θ). Light can only be guided along optical fibers if the incident angle is smaller than this critical angle, giving rise to further coupling losses. When h is larger than the first critical height (denoted as H_2 in Fig. 5 and calculated to be 243 μm), all the incident photons on the fiber would satisfy this condition; the integration limit α_0 will be independent of θ and can be evaluated as

$$\alpha_0 = \frac{1}{2} \left(\arctan \frac{D/2 - r}{h} + \arctan \frac{D/2 + r}{h} \right), \tag{6}$$

where r is the position of the point with respect to the center of the LED (in this model, we assume that the LED consists of numerous point sources of light). On the other hand, as h decreases to another critical height (denoted as H_1 in Fig. 5 and calculated to be 155 μm) as the fiber approaches the LED, the integration limit α_0 begins to be partially dependent on θ and can be evaluated as

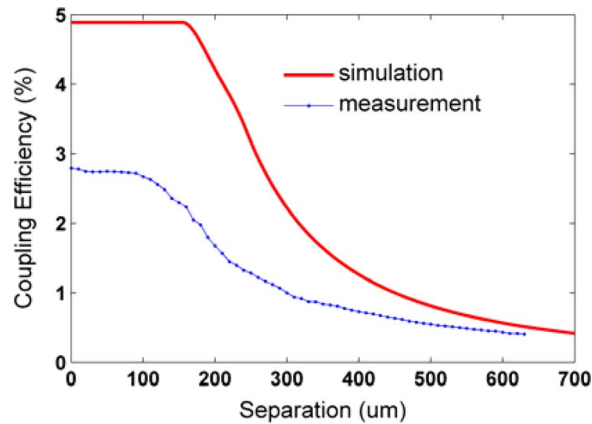$$\alpha_0 = \frac{1}{2} \left(\arctan \frac{D/2 - r}{h} + \theta \right). \tag{7}$$

Fig. 8. The coupling efficiency based on measurement and simulation.

Finally, when $h < H_1$, α_0 is completely determined by the fiber acceptance angle θ, that is,

$$\alpha_0 = \theta. \tag{8}$$

From these equations, the coupling efficiency will be increased with a larger fiber core and with decreasing LED-fiber separation h. In practice, h is limited by the loop height of the bonding wire, which was set to 600 μm when bonding this chip. η was experimentally determined by measuring the optical powers before and after coupling through a single strand of 1 m fiber. At an operation voltage of 3.3 V, the signal emitted from a single pixel was measured as 26.9 μW, and the transmitted power was again measured at the other end at a range separation distance h. h was varied between 0 to 630 μm at intervals of 10 μm. The coupling efficiencies were evaluated by taking the ratio of the optical powers after and before coupling are plotted in the Fig. 8, together with the simulated results based on the model we constructed. From this graph, it can be seen that the trend of the measured results correlates well with the simulated results, although they are consistently lower than the computed values. The lower measured values can be attributed to the deviation between the actual emission pattern and the ideal Lambertian distribution. From Fig. 7, it is observed that more photons are emitted laterally beyond the fiber light acceptance cone than is predicted by the Lambertian function. Additionally, the loss may arise from the experimental setup, such as the accuracy of fiber-LED alignment and the accuracy of determining the separation between them. In fact, this result highlights the advantage of this direct pixel-to-fiber strategy as opposed to the use of an imaging fiber, which would otherwise incur multiple coupling losses. In order to improve light coupling into fibers, the emission patterns from the microscale emitters should be modified in order to increase the extent of overlap with the acceptance cone of the fiber. This can be achieved with fabricated [12] or self-assembled [13] microlenses, which has been proven to be capable of reducing the divergence cone. Another solution involves the integration of a photonic crystal array on top of the emitters [14], [15]. Photonic crystals have been demonstrated to enhance emission directionality. Additionally, surface texturing, such as incorporating pyramidal reflectors on the LED surface, is another effective means of enhancing light extraction [16].

The fraction of emitted light not channeled into its designated fiber may be coupled into the adjacent fiber, contributing to crosstalk. Fortunately, the narrow acceptance cone prevents this from happening. Assuming that the device and fiber bundle are well-aligned, a greater proportion of light will fall into the acceptance cone of the designated fiber as the separation h reduces. As the fiber reaches another critical position denoted as H_3, crosstalk will be completely eliminated. At this point, even photons emitted at the maximum divergence angle will not fall into the acceptance cone of adjacent fibers. H_3 can be calculated based on geometrical considerations as follows:

$$H_3 = ((W - D) + (D - d)/2)/\tan\theta. \tag{9}$$

The calculated value of H_3 for our system is about 333 μm. In our demonstration with $h = 600$ μm, crosstalk might be expected but was not visually observed. From equation (9), it can be deduced that when parameters D, W and θ are fixed for a particular fiber, reducing the pixel dimension d will result in an increase of critical distance H_3 in Fig. 6. Intuitively, designing systems with pixels of smaller dimension and fibers with larger core diameter can facilitate fiber coupling.

4. Conclusion

With a specially-designed optical fiber bundle, a 2-D microdisplay has been demonstrated, using a bi-linear micro-LED array as the display engine. The feasibility of the scheme has been verified by displaying alphanumeric characters at the 2-D end of the fiber bundle. These sharp and clear patterns show that crosstalk can be minimized, if not eliminated, from the fiber-coupled system. Theoretical predictions show that the coupling efficiency can be higher by reducing the LED-fiber separation distance, or the integration of microlenses.

References

[1] H. W. Choi, C. W. Jeon, and M. D. Dawson, "High-resolution 128x96 nitride microdisplay," *IEEE Electron Device Lett.*, vol. 25, no. 5, pp. 277–279, May 2004.
[2] H. Xu, J. Zhang, K. M. Davitt, Y.-K. Song, and A. V. Nurmikko, "Application of blue–green and ultraviolet micro-LEDs to biological imaging and detection," *J. Phys. D, Appl. Phys.*, vol. 41, no. 9, p. 094 013, May 2008.
[3] Y.-L. Pan, V. Boutou, R. K. Chang, I. Ozden, K. Davitt, and A. V. Nurmikko, "Application of light-emitting diodes for aerosol fluorescence detection," *Opt. Lett.*, vol. 28, no. 18, pp. 1707–1709, Sep. 2003.
[4] C. W. Jeon, E. Gu, and M. D. Dawson, "Polymer microlens arrays applicable to AlInGaN ultraviolet micro-light-emitting diodes," *Appl. Phys. Lett.*, vol. 86, no. 22, p. 221 105, May 2005.
[5] Z. Gong, H. X. Zhang, E. Gu, C. Griffin, M. D. Dawson, V. Poher, G. Kennedy, P. M. W. French, and M. A. A. Neil, "Matrix-addressable micropixellated InGaN light-emitting diodes with uniform emission and increased light output," *IEEE Trans. Electron Devices*, vol. 54, no. 10, pp. 2650–2658, Oct. 2007.
[6] L. Campagnola, H. Wang, and M. J. Zylka, "Fiber-coupled light-emitting diode for localized photostimulation of neurons expressing channel-rhodopsin-2," *J. Neurosci. Methods*, vol. 169, no. 1, pp. 27–33, Mar. 2008.
[7] H. Xu, K. M. Davitt, W. Dong, Y.-K. Song, W. R. Patterson, III, C. D. Aizenman, and A. V. Nurmikko, "Combining multicore imaging fiber with matrix addressable blue/green LED arrays for spatiotemporal photonic excitation at cellular level," *IEEE J. Sel. Topics Quantum Electron.*, vol. 14, no. 1, pp. 167–170, Jan./Feb. 2008.
[8] H.-W. Tsao, W.-M. Cheng, and S.-L. Tsao, "Simulation of 4 × 4 light coupling to a single-mode fiber," *Microw. Opt. Technol. Lett.*, vol. 46, no. 2, pp. 103–106, Jul. 2005.
[9] H. W. Choi, E. Gu, J. M. Girkin, and M. D. Dawson, "Nitride micro-display with integrated micro-lenses," *Phys. Stat. Sol. (C)*, vol. 2, no. 7, pp. 2903–2906, May 2005.
[10] Product data sheet, AZ-5214E Image Reversal Photoresist, Clariant Corp., Somerville, NJ, 1990.
[11] H. X. Jiang, S. X. Jin, J. Li, J. Shakya, and J. Y. Lin, "III-nitride blue microdisplay," *Appl. Phys. Lett.*, vol. 78, no. 9, pp. 1303–1305, Feb. 2001.
[12] H. W. Choi, E. Gu, C. Liu, J. M. Girkin, and M. D. Dawson, "Fabrication and evaluation of GaN negative and bifocal microlenses," *J. Appl. Phys.*, vol. 97, no. 6, p. 063 101, Mar. 2005.
[13] Y. K. Ee, R. A. Arif, and N. Tansu, "Enhancement of light extraction efficiency of InGaN quantum wells light emitting diodes using SiO$_2$/polystyrene microlens arrays," *Appl. Phys. Lett.*, vol. 91, no. 22, p. 221 107, Nov. 2007.
[14] A. David, B. Moran, K. McGroddy, E. Matioli, E. L. Hu, S. P. DenBaars, S. Nakamura, and C. Weisbuch, "GaN/InGaN light emitting diodes with embedded photonic crystal obtained by lateral epitaxial overgrowth," *Appl. Phys. Lett.*, vol. 92, no. 11, p. 113 514, Mar. 2008.
[15] T. Kim, A. J. Danner, and K. D. Choquette, "Enhancement in external quantum efficiency of blue light-emitting diode by photonic crystal surface grating," *Electron. Lett.*, vol. 41, no. 20, pp. 1138–1139, Sep. 2005.
[16] J. Q. Xi, H. Luo, A. J. Pasquale, J. K. Kim, and E. F. Schubert, "Enhanced light extraction in GaInN light-emitting diode with pyramid reflector," *IEEE Photon. Technol. Lett.*, vol. 18, no. 22, pp. 2347–2349, Nov. 2006.